2026 IEEE/SICE International Symposium on System Integration (SII)
January 11-14, 2026. Cancún, México

Estimating Wrist Joint Angle using Electromyography and Cepstral Coefficients

Sougo Horimatsu[1], Kensuke Takenaka[1], Takayuki Mukaeda[2,3], and Keisuke Shima[3]

Abstract— **A method was developed for increasing the accuracy of the continuous wrist joint angle estimations for myoelectric prosthetic hands. The method considers cepstral coefficients, which efficiently represent the frequency spectrum characteristics of electromyography (EMG) signals as features. The root mean square myoelectric power (RMS) is conventionally used for myoelectric prosthetic control; however, the sensitivity of the RMS to angle changes is low, especially at the fine muscle contraction level. The proposed method incorporates low-order cepstral coefficients into the feature vector as well as the RMS myoelectric power. This approach increases the angle estimation accuracy through capturing the changes in the spectral shape related to the firing patterns of the motor units. The results of an angle estimation experiment involving wrist dorsiflexion and palmar flexion movements showed that adding a few cepstral coefficients substantially increased the estimation accuracy, particularly when estimating the small flexion angle range. The cepstral coefficient can be used to effectively estimate joint angles from EMG signals, contributing to the development of smoother and more intuitive myoelectric prosthetic control.**

I. INTRODUCTION

The number of upper limb amputees has been increasing annually. A total of 82,000 people had upper limb amputation in 2013 according to a survey by the Cabinet Office of Japan [1]. Furthermore, of the 570 upper limb amputees who responded to a survey questionnaire, 285 (67%) lost their upper limbs due to industrial accidents [2]. Myoelectric prosthetic hands that replicate actual finger movements must be developed because upper limb amputees often experience challenges in performing tasks requiring dexterous finger movements. Myoelectric prosthetic hands estimate motion using electromyogram (EMG) signals to reproduce the intended movements of the user. Numerous methods use only EMG signals to control prosthetic hands [3]–[5]. Other methods combine EMG with other biological information, such as image recognition technology for identification [6], or use logistic regression for threshold-based discrimination [7]. However, human fingers have many degrees of freedom, and the EMG signals that can be measured from the forearm or upper arm are limited. Therefore, completely estimating human finger movements using EMG signals alone is difficult [8]. Impedance can also be used for controlling myoelectric prostheses, which enables the flexible movements of the human arm [4]. Furui et al. proposed an angle control method based on the λ model, which mimics human impedance control characteristics, to produce smoother, more life-like movements [9]. These methods primarily use the root mean square myoelectric power (RMS) as a feature to reflect the degree of muscle contraction. However, the RMS effectively captures the overall magnitude of muscle contraction; however, the sensitivity is insufficient for fine force control and small joint angle changes. However, the frequency spectrum of EMG signals contains more detailed muscle activity information, such as the shape and firing frequency of the active motor units (MUs). Cepstrum analysis has been considered to effectively use this frequency spectrum information. Cepstrum analysis represents the general shape of a spectrum using a small number of parameters. Cepstral coefficients are features of EMG signals that have mainly been applied in pattern recognition problems for classifying arm or finger movements [10]–[12]. However, cepstral coefficients have not been applied to the regression problem of estimating continuous joint angles: joint angles must be continuously estimated for smoothly controlling prosthetic hands. Therefore, a method was developed that includes the cepstral coefficients as a feature in addition to the conventional RMS for continuous wrist joint angle estimation. This coefficient captures the shape of the frequency spectrum. The entire frequency spectrum cannot be directly used as the input for myoelectric prostheses, which require real-time control, because the dimensionality of the features is too large. A hypothesis was formulated and tested to determine whether incorporating low-dimensional cepstral coefficients into the model would increase the estimation accuracy while retaining important information in the spectrum. The remainder of this paper is organized as follows. Section II describes related work. Section III explains the angle estimation method. Section IV presents the experimental conditions for validating the proposed method, along with the results and discussion.

II. RELATED WORK

As an approach to utilizing the frequency spectrum information of EMG signals, a method that treats spectrograms obtained by Short-Time Fourier Transform (STFT) as images and inputs them into a Convolutional Neural Network (CNN) has recently attracted attention. Benavides-Álvarez et al. reported achieving 100% accuracy in the classification of six basic grasping motions by converting EMG signals into spectrogram images for each channel and inputting them into a custom-designed CNN model [13]. Similarly, Côté-Allard et al. and Raza et al. have demonstrated the effectiveness

[1]Graduate School of Environment and Information Sciences, Yokohama National University, 79-5 Tokiwadai, Hodogaya-ku, Yokohama, Japan
[2]Kanagawa Institute of Industrial Science and Technology, 705-1 Shimoimaizumi, Ebina, Kanagawa, Japan
[3]Faculty of Environment and Information Sciences, Yokohama National University, 79-5 Tokiwadai, Hodogaya-ku, Yokohama, Japan

978-1-6654-5784-2/26/$31.00 ©2026 IEEE

of this approach by achieving high classification accuracy by combining spectrogram images and CNNs [14], [15]. However, when using spectrograms directly as input, the data format becomes high-dimensional image data, resulting in an enormous number of features. Côté-Allard et al. pointed out that STFT alone generates a large number of features and that the computational cost is relatively high [14]. This remains a challenge for control applications in myoelectric prostheses where real-time performance is strictly required. This study, therefore, focuses on validating the effectiveness of CCs themselves as features using a lightweight linear model (Ridge Regression), rather than pursuing the high accuracy of computationally expensive models like DL. As a means of utilizing frequency spectrum information while avoiding this computational cost issue, cepstrum analysis can be mentioned. Cepstral coefficients are features that efficiently represent the general shape information of the spectrum with low-dimensional parameters. Yoshikawa et al. introduced cepstral coefficients as features in finger posture estimation from EMG signals and showed that the accuracy of motion classification by SVM improved [16]. The authors stated that cepstral coefficients are effective for achieving robust classification with low-dimensional vectors. However, this research focused on the classification of discrete motions, and no studies have directly applied cepstral coefficients to the regression problem of estimating continuous joint angles, an application essential for the smooth control of prosthetic hands.

III. ANGLE ESTIMATION METHOD

In this paper, wrist joint angles are estimated by calculating multiple features from EMG signals and inputting them into a linear regression model. This section details the signal processing leading to feature calculation, the definition of each feature, and the angle estimation model.

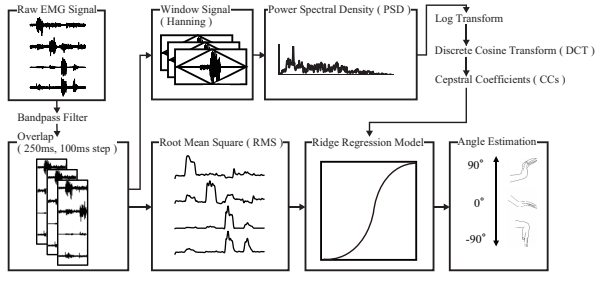

Fig. 1. Signal processing pipeline for angle estimation.

A. Signal Processing

Raw EMG signals measured from D channels on the forearm at a sampling frequency of $f_s = 1000$ Hz are first processed with a 2nd-order Butterworth bandpass filter (cutoff frequencies: 20-450 Hz) to obtain a signal $e(t)$ with noise and motion artifacts removed. All subsequent feature calculations are based on this filtered signal $e(t)$.

B. Feature Extraction

From the signal $e(t)$, the following features are calculated for each channel within an analysis window of width $N = 250$ samples (250 ms), with an overlap of 150 samples (step size 100 ms).

1) Power Spectrum Calculation: To calculate frequency-domain features, the Power Spectral Density (PSD) is first estimated from the signal $e(n)$ within each analysis window. To reduce signal leakage error, a Hanning window $w(n)$ is first applied to the N-point signal $e(n)$.

$$e_w(n) = e(n) \cdot w(n), \quad n = 1, \ldots, N \tag{1}$$

Subsequently, the periodogram method is used to calculate the PSD $P(f)$ from the windowed signal $e_w(n)$.

$$P(f) = \frac{1}{f_s N} \left| \sum_{n=1}^{N} e_w(n) e^{-j2\pi f n / f_s} \right|^2 \tag{2}$$

The MNF, cepstral coefficients, and PSdiv, described below, are all calculated using this PSD $P(f)$.

2) Root Mean Square (RMS): As the most fundamental feature reflecting the intensity of muscle activity, the RMS is calculated from the signal $e(n)$ within the analysis window using the following equation.

$$\text{RMS} = \sqrt{\frac{1}{N} \sum_{n=1}^{N} e(n)^2} \tag{3}$$

3) Mean Frequency (MNF): As an index representing the centroid of the frequency spectrum, an index said to reflect effects such as muscle fatigue, the MNF is calculated using the following equation.

$$\text{MNF} = \frac{\sum_{j=1}^{M} f_j P(f_j)}{\sum_{j=1}^{M} P(f_j)} \tag{4}$$

Here, f_j is the j-th frequency bin, and M is half the number of FFT points.

4) Cepstral Coefficients (CC): To represent the information of the spectral envelope in a low-dimensional form, real cepstral coefficients are calculated. The cepstrum $C(q)$ is obtained by taking the logarithm of the power spectral density $P(f)$ and then applying the Discrete Cosine Transform (DCT), an inverse Fourier transform that returns real values.

$$C(q) = \mathcal{F}_{\text{DCT}}\{\log |P(f)|\} \tag{5}$$

Here, $\mathcal{F}_{\text{DCT}}$ represents the Discrete Cosine Transform, and q is a pseudo-time domain dimension called quefrency. In this study, the low-order cepstral coefficients $CC_k = C(k)$ for $k = 1, \ldots, 5$ are used as features.

5) Power Spectrum Division (PSdiv): As a feature that more directly inputs the overall shape information of the spectrum, the power spectrum is divided into multiple frequency bands, and the average power of each band is calculated. For comparison, in this study, the power spectral density $P(f)$ is divided equally into 10 or 20 bands, and their respective average powers are used as the feature sets PS10div and PS20div.

C. Angle Estimation using Ridge Regression

This study employs Ridge Regression as the estimator to map the feature vector to the joint angle. Ridge Regression is a linear regression model that introduces an L2 regularization term, enabling robust estimation when the number of features is large compared to the number of samples or when there is strong correlation (multicollinearity) among the features. Let the input feature vector be $\boldsymbol{x} \in \mathbb{R}^d$, the estimated angle be $y \in \mathbb{R}$, the weight vector be $\boldsymbol{w} \in \mathbb{R}^d$, and the bias be $b \in \mathbb{R}$. Ridge Regression minimizes the following cost function $J(\boldsymbol{w}, b)$.

$$J(\boldsymbol{w}, b) = \frac{1}{m} \sum_{i=1}^{m} ((\boldsymbol{w}^T \boldsymbol{x}^{(i)} + b) - y^{(i)})^2 + \alpha \sum_{j=1}^{d} w_j^2 \quad (6)$$

Here, m is the number of training samples, and $\alpha \geq 0$ is a hyperparameter that determines the strength of the regularization. This model was selected for its versatility and ease of implementation to validate the effectiveness of the features.

IV. EXPERIMENTS

To comprehensively validate the effectiveness of the proposed method, a wrist joint angle estimation experiment was designed. This paper first conducts several basic experiments focusing on specific motion elements (e.g., maintaining an angle, continuous angle changes) to analyze the estimation accuracy when using cepstral coefficients as features and the mechanisms contributing to this accuracy improvement.

A. Experimental Conditions

The measurement system used in this experiment is shown in Fig. 2. Three healthy male subjects in their 20s participated, performing the movements while seated with their elbows on a desk. For EMG signal measurement, a total of $D = 4$ channels of wet surface electrodes were attached: two channels each on the muscles used for dorsiflexion (e.g., extensor digitorum communis, extensor carpi ulnaris) and palmar flexion (e.g., flexor carpi radialis) of the forearm (Fig. 2(a)). The sampling frequency during measurement was $f_s = 1000$ Hz. The wrist joint angle was measured with a goniometer attached to the subject's wrist. The biosignalsplux system (Creact) was used to acquire both EMG and angle signals (Fig. 2(b)). The analysis window width for feature calculation was $T_w = 250$ ms ($N = 250$ samples), and the window shift was $T_s = 100$ ms.

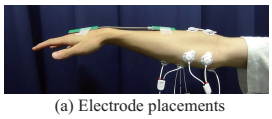

(a) Electrode placements

(b) Biosignalsplux

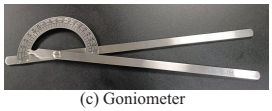

(c) Goniometer

Fig. 2. Measurement system. (a) Electrode placements, (b) Biosignalsplux, (c) Goniometer.

The subjects were instructed to align their wrist angle with a target angle indicated by the needle of a goniometer (Shinchu-shiki, Collaborates Inc.) placed on the desk. The experimental setup is shown in Fig. 3. The resting state was set as the baseline (0%), and tasks were structured using relative angles, with the pre-measured maximum dorsiflexion and palmar flexion angles defined as 100%, respectively.

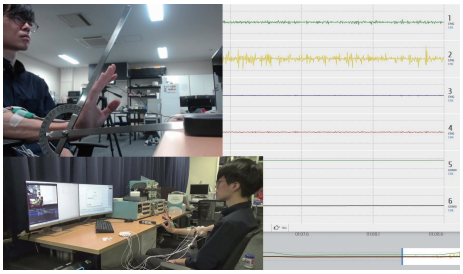

Fig. 3. Experimental scene.

1) Measurement 1: Angle Hold Task: To evaluate estimation accuracy during static posture maintenance, subjects were instructed to maintain a specified angle for a certain period. The task consisted of a cycle: transition from a resting state to a specified angle (25%, 50%, 75%, 100% of maximum flexion) in 1 second, holding for 3 seconds, then returning to the resting state in 1 second and holding for 3 seconds (Fig. 4(a)). This was performed for 10 trials each for dorsiflexion and palmar flexion.

2) Measurement 2: Continuous Angle Change Task: To evaluate the ability to track dynamic angle changes, subjects were instructed to move their wrist continuously between maximum dorsiflexion and maximum palmar flexion at a constant speed (approximately one round trip per second) from a resting state (Fig. 4(b)). This movement was repeated for 10 trials.

3) Measurements 3 & 4: Step-and-Hold Tasks: To evaluate performance in situations where static and dynamic states alternate, subjects were instructed to repeat a motion of transitioning to a specified angle in 1 second and holding for 3 seconds in a stepwise manner. In Measurement 3, the angle was changed in 25% increments (Fig. 4(c)), and in Measurement 4, in 50% increments (Fig. 4(d)). Each task was performed for 10 trials.

To evaluate the contribution of features to angle estimation accuracy, the following nine feature sets are compared.

- **A**: RMS
- **B**: RMS + MNF
- **C**: RMS + CC_1
- **D**: RMS + $CC_1 \sim CC_2$
- **E**: RMS + $CC_1 \sim CC_3$
- **F**: RMS + $CC_1 \sim CC_4$
- **G**: RMS + $CC_1 \sim CC_5$
- **H**: RMS + PS10div
- **I**: RMS + PS20div

To robustly evaluate the generalization performance of the model, 5-fold cross-validation was employed. For each measurement task, the pairs of feature and angle data obtained

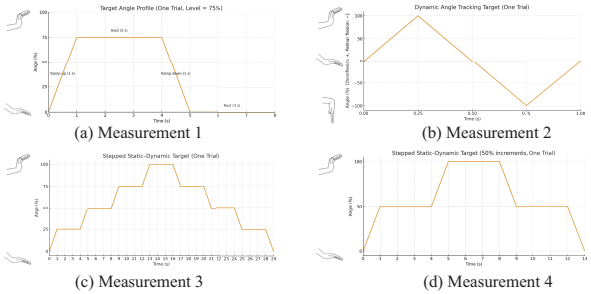

Fig. 4. Time-series trajectories of the target angle for each measurement task. (a) Measurement 1: Angle hold task (example at 75%), (b) Measurement 2: Continuous angle change task, (c) Measurement 3: Step-and-hold task (25% steps), (d) Measurement 4: Step-and-hold task (50% steps).

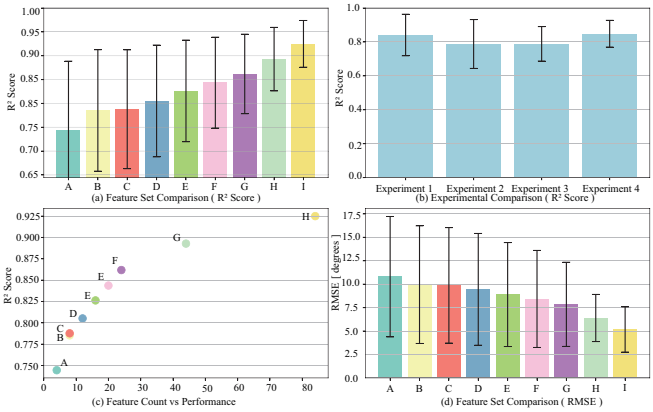

Fig. 5. Overall estimation performance. (a) R^2 score for each feature set, (b) R^2 score for each experimental condition, (c) Relationship between the number of features and performance, (d) RMSE for each feature set.

from all trials were randomly divided into five groups (folds). A Ridge Regression model was trained using four of these groups as training data, and the remaining group was used as evaluation data. This process was repeated five times. The final evaluation metric was the average of the values obtained from the five trials. The evaluation metrics used were the Root Mean Square Error (RMSE) and the coefficient of determination (R^2 score). For m evaluation data points, with the measured angle as $y^{(i)}$ and the model's estimated angle as $\hat{y}^{(i)}$, the RMSE is defined by the following equation.

$$\mathrm{RMSE} = \sqrt{\frac{1}{m}\sum_{i=1}^{m}(y^{(i)} - \hat{y}^{(i)})^2} \tag{7}$$

Furthermore, as an index showing how well the model can explain the variance of the data, the R^2 score is defined by the following equation.

$$R^2 = 1 - \frac{\sum_{i=1}^{m}(y^{(i)} - \hat{y}^{(i)})^2}{\sum_{i=1}^{m}(y^{(i)} - \bar{y})^2} \tag{8}$$

Here, $\bar{y}$ is the average of the measured angles.

B. Results

The results of this experiment confirmed that adding cepstral coefficients as features, as proposed, leads to a statistically significant improvement in estimation accuracy. This section first quantitatively evaluates the overall estimation accuracy and feature efficiency, followed by a detailed analysis and discussion of the mechanism behind this accuracy improvement.

1) Evaluation of Estimation Accuracy and Efficiency: Fig. 5 shows the relationship between the average estimation accuracy and efficiency for each feature set, calculated across all measurement tasks.

As shown by the RMSE in Fig. 5(d) and the R^2 score in Fig. 5(a), all feature sets that added some form of frequency feature to RMS (B through I) significantly improved the estimation error compared to the baseline using only RMS (A) ($p < 0.05$). This confirms the universal effectiveness of adding EMG signal frequency information to angle estimation. Next, the efficiency of performance improvement is considered. Fig. 5(c) plots each set with the number of features on the horizontal axis and the R^2 score on the vertical axis. The highest accuracy was shown by feature set I (RMS + PS20div), but its feature dimensionality is very large at 84 dimensions. On the other hand, focusing on the feature sets with added cepstral coefficients (C through G), a trend of steady accuracy improvement is observed as the number of features increases. As shown in Table I, the RMSE steadily decreases as features are added. In particular, cepstral coefficients can be said to be an efficient index in that they can improve accuracy incrementally with fewer dimensions compared to PSdiv, which uses the entire spectrum.

TABLE I
FEATURE DIMENSIONS AND AVERAGE RMSE FOR ALL FEATURE SETS.

Feature Set	No. of Features	Avg. RMSE [deg]
A: RMS	4	10.80
B: RMS, MNF	8	9.95
C: RMS, CC_1	8	9.88
D: RMS, $CC_1 \sim CC_2$	12	9.45
E: RMS, $CC_1 \sim CC_3$	16	8.90
F: RMS, $CC_1 \sim CC_4$	20	8.43
G: RMS, $CC_1 \sim CC_5$	24	7.85
H: RMS, PS10div	44	6.39
I: RMS, PS20div	84	5.17

To further analyze the contribution of CCs, an ablation study on the number of coefficients was conducted. As shown in Fig. 6, the estimation accuracy (R^2 score) improves significantly as the first few CCs are added. The performance continues to rise steadily up to 10 orders.

Furthermore, to analyze repeatability, the relationship between the number of training trials and estimation accuracy was evaluated. Fig. 7 shows that the estimation accuracy remains high and stable even when trained on a small number of trials (e.g., 3-4 trials), demonstrating the method's robustness and trial-to-trial consistency.

2) Discussion of the Accuracy Improvement Mechanism: To investigate the mechanism by which frequency features,

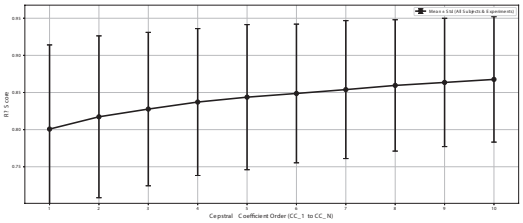

Fig. 6. Cepstral Coefficient order vs R^2 score (Averaged over all subjects and experiments).

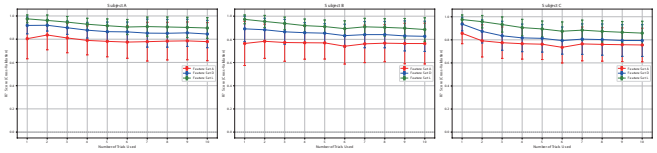

Fig. 7. Trial count vs estimation accuracy (R^2 score) by subject.

especially cepstral coefficients, contribute to accuracy improvement, the behavior of the features was analyzed in detail. Fig. 8 shows two EMG signal segments (states A and B) where the muscle activity level is nearly identical (very similar RMS values) but the muscle contraction states are different, along with the various features calculated from them.

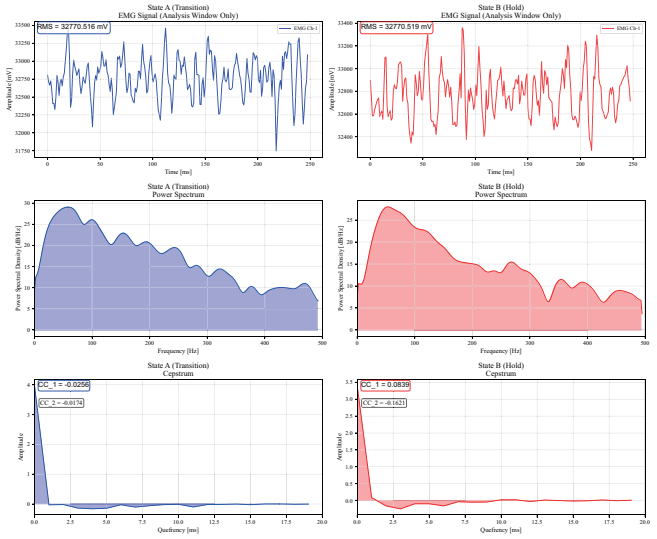

Fig. 8. Example of feature extraction from two different EMG signal states with similar RMS values. While RMS values are nearly identical, the power spectra exhibit different shapes, which are effectively captured by the distinct values of the low-order Cepstral Coefficients.

Even for these states that are indistinguishable by RMS, looking at the power spectrum reveals that their shapes, particularly the proportion of low-frequency components, are different. The cepstral coefficients acutely capture this difference in spectral shape and show clearly distinct values. This fact is particularly important in tasks involving holding a small flexion angle and at the onset of movement. In these situations, the total amount of muscle activity (RMS) may be similar between a state of moving the angle (Transition phase) and holding it (Hold phase), but the spectral shape reflecting the muscle's control state is different. When only RMS is used as a feature, this difference cannot be captured, leading to estimation errors. In contrast, since cepstral coefficients can distinguish this change in state, they lead to robust estimation, especially at low muscle contraction levels, and are thought to contribute significantly to accuracy improvement. This characteristic can also be confirmed in a time-series view. Fig. 9 shows the response of RMS and cepstral coefficients in a task at a low muscle contraction level. In the state of holding the angle (Hold phase), a tendency for the RMS value to decrease compared to the state of changing the angle (Transition phase) was observed. On the other hand, the cepstral coefficients showed more stable values regardless of the muscle's contraction state (dynamic or static). This stability is considered to contribute to the improvement in estimation accuracy.

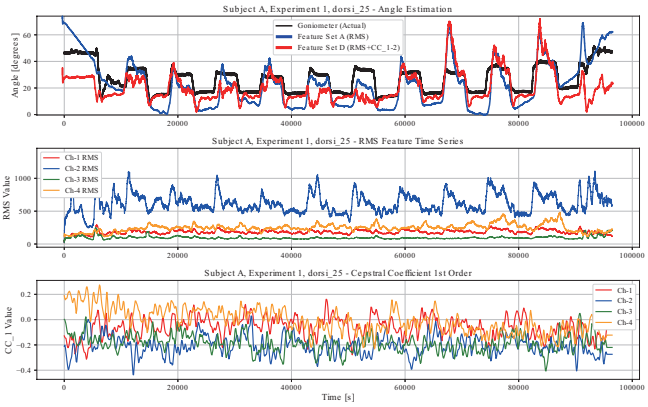

Fig. 9. Time-series response of RMS and Cepstral Coefficient (CC_1) during a low flexion angle task.

In the EMG signal spectrum, high-frequency components above 40 Hz are said to primarily reflect the shape information of Motor Unit Action Potentials (MUAPs) (the number of active motor units), while low-frequency components below 40 Hz are said to reflect the influence of firing patterns such as firing frequency. In the example in Fig. 8, the proportion of power in the low-frequency region below 40 Hz is particularly different. Precise muscle tension control, i.e., angle control, is performed not only by increasing the number of participating motor units (recruitment) but mainly by changing the firing frequency. Since cepstral coefficients can capture this overall change in spectral shape, especially the change in the low-frequency region, it can be inferred that they are able to supplement the features of MUAP firing patterns that cannot be captured by RMS alone.

3) Visualization of Estimation Results with a Virtual Hand: To demonstrate the potential of the proposed method to achieve intuitive control in practical applications such as prosthetic hands, a simulation was conducted to drive a virtual hand using the estimated angles. As shown in Fig. 10, the correspondence between the subject's actual wrist flexion angles and the virtual hand's movements based on the offline

estimated angles from the measured data is excellent. This confirms that the proposed method leads to visually smooth and accurate control.

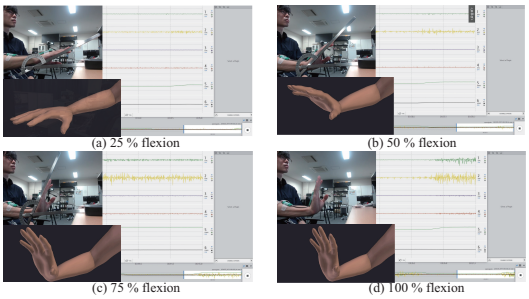

Fig. 10. Correspondence between the subject's actual wrist postures and the virtual hand driven by the estimated angles at different flexion levels: (a) 25%, (b) 50%, (c) 75%, and (d) 100% dorsiflexion.

V. CONCLUSION

A method was developed to increase the accuracy when estimating continuous joint angles for myoelectric prostheses. The method includes cepstral coefficients as features. The effectiveness of the model was verified through multiple experimental tasks. Adding this frequency feature to the RMS substantially increases the joint angle estimation accuracy. Feature set G (24 dimensions) added cepstral coefficients to the RMS, increasing the average RMSE from 10.80° to 7.85° compared with that of the baseline (RMS only, four dimensions). The efficiency of the method was evaluated using the amount the RMSE decreased per added dimension. Adding cepstral coefficients reduced the RMSE by approximately 0.148°/dimension. This is more than double the increase in efficiency achieved with the highest-accuracy feature set I (84 dimensions) (approximately 0.070°/dimension). This finding quantitatively shows that the cepstral coefficient is an efficient feature in this estimation. Adding cepstral coefficients increases estimation accuracy by precisely capturing the changes in spectral shape caused by motor unit firing patterns, which cannot be captured by the RMS, particularly at low muscle contraction levels. We will address the limitations of this study in future studies, namely, the small number of subjects (three) and the restriction of experiments to simple tabletop tasks, by increasing the participant pool and conducting testing under more complex experimental conditions. Able-bodied individuals were targeted in this study; the future aim is to apply the developed model in people with upper-limb amputation. Furthermore, the robustness of the model against practical challenges, such as electrode shifting and muscle fatigue, must be evaluated. Therefore, a system that controls the joint angle corresponding to the intended muscle contraction level of the person must be constructed to manage situations in which the ground-truth joint angle cannot be obtained. Furthermore, this study was limited to an offline analysis; future research will involve applying the model with an actual robotic hand and verifying its effectiveness in real-time control. The CCs validated in this study may be integrated as features into more advanced deep learning models (e.g., CNNs) to further increase estimation accuracy. The goal of addressing these challenges is to enable more intuitive and practical myoelectric prosthetic control to increase the quality of life of people with prosthetic limbs.

REFERENCES

[1] Cabinet Office, Japan, "Status of children and adults with disabilities," *White Paper on Persons with Disabilities, Heisei 25*, vol. Appendix, no. 8, 2013.

[2] J. Kawamura, N. Fukui, M. Nakagawa, T. Fujishita, T. Aoyama, and H. Furukawa, "Current status and trends of upper limb amputees: From a questionnaire survey in the kinki district," *Japanese Journal of Rehabilitation Medicine*, vol. 36, no. 6, pp. 384–389, 1999.

[3] A. Furui, S. Eto, K. Nakagaki, K. Shimada, G. Nakamura, A. Masuda, T. Chin, and T. Tsuji, "A myoelectric prosthetic hand with muscle synergy-based motion determination and impedance model-based biomimetic control," *Science Robotics*, vol. 4, no. 31, p. eaaw6339, 2019.

[4] T. Tsuji, O. Fukuda, H. Shigeyoshi, and M. Kaneko, "Bio-mimetic impedance control of an emg-controlled prosthetic hand," *IEEE/RSJ International Conference on*, vol. 1, pp. 377–382, 2000.

[5] Ito, Nagaoka, Tsuji, Kato, and Ito, "3-dof forearm emg prosthetic hand using ultrasonic motor," *Transactions of the Society of Instrument and Control Engineers*, vol. 27, no. 11, pp. 1281–1289, 1991.

[6] P. Shi, K. Fang, and H. Yu, "Design and control of intelligent bionic artificial hand based on image recognition," *TECHNOLOGY AND HEALTH CARE*, vol. 31, no. 1, pp. 21–35, 2023.

[7] F. Leone, C. Gentile, F. Cordella, E. Gruppioni, E. Guglielmelli, and L. Zollo, "A parallel classification strategy to simultaneous control elbow, wrist, and hand movements," *JOURNAL OF NEUROENGINEERING AND REHABILITATION*, vol. 19, no. 1, JAN 28 2022.

[8] C. Igual, L. A. Pardo, J. M. Hahne, and J. Igual, "Myoelectric control for upper limb prostheses," *Electronics*, vol. 8, no. 11, 2019. [Online]. Available: https://www.mdpi.com/2079-9292/8/11/1244

[9] A. Furui, K. Nakagaki, and T. Tsuji, "Biomimetic control of myoelectric prosthetic hand based on a lambda-type muscle model," *arXiv preprint arXiv:2105.14215*, 2021, available online. [Online]. Available: https://arxiv.org/abs/2105.14215

[10] M. Yoshikawa, M. Mikawa, and K. Tanaka, "Real-time hand motion identification by support vector machine using myoelectric signals (welfare engineering)," *IEICE TRANSACTIONS on Information and Systems*, vol. 92, no. 1, pp. 93–103, 01 2009. [Online]. Available: https://cir.nii.ac.jp/crid/1050282677616853888

[11] M. Yoshikawa, Y. Mita, M. Mikawa, and K. Tanaka, "A fundamental study on a hand motion identification method for forearm amputees using emg signals," *The Japanese Journal of Ergonomics*, vol. 46, no. 3, pp. 197–207, 2010. [Online]. Available: https://cir.nii.ac.jp/crid/1390001204538394240

[12] K. Ishikawa, M. Toda, S. Sakurazawa, J. Akita, K. Kondo, and Y. Nakamura, "A wearable music interface using surface electromyography signals," *The Journal of The Society for Art and Science*, vol. 11, no. 2, pp. 12–20, 2012.

[13] C. Benavides-Alvarez, E. Rodríguez-Martínez, C. Avilés-Cruz, A. Zúñiga López, A. Ramírez, and M. Aguilar-Sánchez, "Improvement in the classification of emg signals through a convolutional neural network," *Neural Computing and Applications*, vol. 37, pp. 20 299–20 313, 07 2025.

[14] U. Côté Allard, C. L. Fall, A. Drouin, A. Campeau-Lecours, C. Gosselin, K. Glette, F. Laviolette, and B. Gosselin, "Deep learning for electromyographic hand gesture signal classification using transfer learning," *IEEE transactions on neural systems and rehabilitation engineering: a publication of the IEEE Engineering in Medicine and Biology Society*, vol. PP, 01 2019.

[15] M. F. Qureshi, Z. Mushtaq, M. Z. U. Rehman, and E. N. Kamavuako, "E2cnn: An efficient concatenated cnn for classification of surface emg extracted from upper limb," *IEEE Sensors Journal*, vol. 23, no. 8, pp. 8989–8996, 2023.

[16] M. Yoshikawa, M. Mikawa, and K. Tanaka, "Hand pose estimation using emg signals," *Conference proceedings : ... Annual International Conference of the IEEE Engineering in Medicine and Biology Society. IEEE Engineering in Medicine and Biology Society. Conference*, vol. 2007, pp. 4830–3, 02 2007.